PLOS ONE

Darcy-Forchheimer hybrid nanofluid flow over a stretching curved surface with heat and mass transfer

Anwar Saeed[1], Wajdi Alghamdi[2], Safyan Mukhtar[3], Syed Imad Ali Shah[4], Poom Kumam[1,5]*, Taza Gul[4], Saleem Nasir[6], Wiyada Kumam[7]

1 Faculty of Science, Center of Excellence in Theoretical and Computational Science (TaCS-CoE), King Mongkut's University of Technology Thonburi (KMUTT), Thung Khru, Bangkok, Thailand, **2** Faculty of Computing and Information Technology, Department of Information Technology, King Abdulaziz University, Jeddah, Saudi Arabia, **3** Department of Basic Sciences, Deanship of Preparatory Year, King Faisal University, Hofuf, Al Ahsa, Saudi Arabia, **4** Mathematics Department, City University of Science and Information Technology, Peshawar, Pakistan, **5** Department of Medical Research, China Medical University Hospital, China Medical University, Taichung, Taiwan, **6** Department of Mathematics, Abdul Wali Khan University, Mardan, Khyber, Pakhtunkhwa, Pakistan, **7** Faculty of Science and Technology, Department of Mathematics and Computer Science, Program in Applied Statistics, Rajamangala University of Technology Thanyaburi, Thanyaburi, Pathumthani, Thailand

* poom.kum@kmutt.ac.th

OPEN ACCESS

Abstract

The present article provides a detailed analysis of the Darcy Forchheimer flow of hybrid nanoliquid past an exponentially extending curved surface. In the porous space, the viscous fluid is expressed by Darcy-Forchheimer. The cylindrical shaped carbon nanotubes (SWCNTs and MWCNTs) and Fe_3O_4 (iron oxide) are used to synthesize hybrid nanofluid. At first, the appropriate similarity transformation is used to convert the modeled nonlinear coupled partial differential equations into nonlinear coupled ordinary differential equations. Then the resulting highly nonlinear coupled ordinary differential equations are analytically solved by the utilization of the "Homotopy analysis method" (HAM) method. The influence of sundry flow factors on velocity, temperature, and concentration profile are sketched and briefly discussed. The enhancement in both volume fraction parameter and curvature parameter k results in raises of the velocity profile. The uses of both Fe_3O_4 and CNTs nanoparticles are expressively improving the thermophysical properties of the base fluid. Apart from this, the numerical values of some physical quantities such as skin friction coefficients, local Nusselt number, and Sherwood number for the variation of the values of pertinent parameters are displayed in tabular forms. The obtained results show that the hybrid nanofluid enhances the heat transfer rate 2.21%, 2.1%, and 2.3% using the MWCNTs, SWCNTs, and Fe_3O_4 nanomaterials.

1. Introduction

The flow analysis over a stretch sheet is essential for use in many engineering and industrial sectors. Its fascinating applications are utilized in the production of plastic and rubber sheets, metalworking processes such as hot rolling, aerodynamic extrusion of plastic sheets, melt spinning as a metal forming technique, elastic polymer substance, and emollient production, paints, production of glass-fiber, etc. The first analysis on the flow overextending plane surface was made by Crane [1]. Generally, Crane's suggested model of the linearly stretching plate is not used in many industrial sectors. So, researchers find an interest in investigating the various aspects of the stretching rate. Later on, following Crane's idea, many researchers investigate several characteristics of this type of flow over the stretching sheet [2]. Sajid et al. [3] contemplated micropolar fluid and boundary layer flow and concluded that the dimensionless curvature results in the improvement of the layer size. Imtiaz et al. [4] illustrated MHD flow with heterogeneous-homogeneous reactions due to the stretching curved surface. It is evident that the temperature and velocity of fluid rise for higher curvature. Rosca et al. [5] examined fluid flow due to contracting and extending sheets. Hayat et al. [6] numerically investigated the Darcy-Forchhemier flow of extending bent surface with Cattaneo-Christov theory. Kumar et al. [7] deliberated the radiation effect on MHD fluid (Casson) flow over the exponentially curved sheet. Hayat et al. [8] and Maria et al. [9] investigate ferro liquid flow with homogeneous-heterogeneous effect over the curled widening surface. The viscous fluid flow with the power-law over the extending bent surface was examined by Sanni et al. [10]. The nano-silver and diamond thermos physical characteristics simulations over curved surface flow were investigated by Khan et al. [11]. Some other relevant and innovative investigations under different conditions are discussed in [12–15].

Nanofluids have attracted significant interest from researchers due to their motivating heat transfer in numerous manufacturing and engineering applications. Traditional operating fluids such as water, engine oils, and ethylene glycol have reduced thermal efficiency that restricts their use in modern cooling applications. Nanofluids comprise nanoparticles such as copper, alumina, carbides, nitrides, metal oxides, graphite, and carbon nanotubes that improve the thermal conductivity of base fluids. These nanofluids are commonly used in modern heating and cooling systems, solar panels, the latest fuel generation, hybrid-powered vehicles, cancer treatment, drug delivery, and medicine. A variety of experiments related to the flow of nanofluids have been performed due to these various applications of nanofluids. Thermal conductivity and convective heat transfer are enhanced by the suspension of nanoparticles in the base fluid. Choi [16] initially adopted this concept and introduced a revolutionary new form of nanofluid that represents high thermal conductivity.

The heat transfer of nano-carbon fluid has received considerable interest in the last two decades due to its extensive uses in the fields of nanotechnology and medicine. CNTs are the simple chemical structure along with the composition of carbon atoms, rolled in cylindrical form. CNTs have extraordinary thermophysical, chemical, electrical, and mechanical features that can be utilized efficiently as a nanoparticle in the base fluid. They have unique advantages because of tiny tube-sized structures, such as large surface area, configuration, chemical stability, hardness, and their smallest dimension over other nanoparticles. CNTs depend on the number of graphene layers, which subdivided it into (SWCNTs) single-walled and (MWCNTs) multi-walled carbon nanotubes, respectively. Haq et al. [17] examined the numerical outcomes for conducting fluid and heat exchange due to carbon nanotubes merged in various based fluids over an extending sheet using a numerical scheme. The influence of carbon nanotubes water-based nano liquid (micropolar) on heat transport and magneto-hydrodynamics (MHD) flow between two rotating discs using the HAM technique was employed by

Rahman et al. [18]. Mathanthash et al. [19] studied the heat source's impact and exponential space during the nanofluid Flow. The entropy generation between two rotating disks of CNTs nanofluid flow in the occurrence of thermal radiation and MHD was inspected by Hosseinzedeh et al. [20]. Ding et al. [21] explored the heat transfer using (MWCNTs) in the base liquid. Akber et al. [22] described the magnetic field's influence over CNTs nanofluid flow through a moving permeable channel.

Hybrid nanofluids have become a new class of working fluids that comprise extremely small particles less than 100 nm in size and are important in heat transfer applications. These fluids consist of two solid materials, such as Al_2O_3–Cu, SWCNTs-Fe_3O_4, MWCNTs-Fe_3O_4, Al_2O_3–Ag, Cu–TiO_2 and Cu–CuO, in traditional liquids (water, kerosene, ethylene glycol, and engine oil). The purpose of the use of hybrid nanofluids is to further improve the flow of heat and grow nanotechnology. Nowadays, these hybrid nanofluids are implemented in numerous heat transfer applications as mini channel heat sinks, air conditioning systems, micro channels, helical coil heat exchangers, tubular and plate heat exchangers. An extensive research on hybrid nanofluids can be found in the literature for example Gabli et al. [23] have examined the Fe_3O_4 nanoparticles dispersion in the non-Newtonian fluids for heat transfer enhancement. The status of hybrid nanofluid in the heat development rate has been premeditated by Nadeem et al. [24]. Chamkha et al. [25] scrutinized the transmission of heat and magnetohydrodynamic Flow of hybrid nanofluids utilizing a rotating frame. Sundar et al. [26] explored the heat transfer features of Graphene Oxide /CO_3O_4 hybrid nanofluids. Wei et al. [27] estimated the thermophysical properties of oil-based hybrid nanofluids for heat transferal uses. Momin [28] investigated analytically the various aspects of diverse convective laminar hybrid nanoliquid flow in a tending cylinder. Sundar et al. [29] inspected the greater temperature energy transfers and the friction feature of the hybrid nano liquid. Some latest studies on different flow geometries of hybrid nanofluid are listed in Refs. [30–33].

The novelty of the model is pointed out as:

- The heat and mass transfer at the same time for the solid nanoparticles initiated, while in the existing literature, only the heat transfer is considered.

- The (CNT_S+Fe_3O_4/H_2O) hybrid nanofluid flow due to an extending surface for the heat and mass transfer is considered while no one has considered the (CNT_S+Fe_3O_4/H_2O) hybrid nanofluid for the same model.

- Our motivation for the current work, to investigate and model the Darcy-Forchheimer water-based (CNT_S+Fe_3O_4) hybrid nano liquid flow due to an extending curved surface.

- The priority to initiate the Xue [34] and Saba et al. [35] theoretical models for such type of Flow and set up an arrangement for velocity and the temperature profile opted "Homotopy analysis method" (HAM).

- We have protracted the idea of Hayat et al. [36] by including the above-mentioned features.

2. Problem formulation

Let us consider the steady and two-dimensional Darcy Forchheimer flow of hybrid nano liquid due to an extending curved surface. In permeable space, the viscous fluid is expressed by Darcy-Forchheimer. The flow is induced through the exponential folded sheet, spiral in a circle with radius R, illustrated in Fig 1. Here (u, v) is taken as the velocity component and (r, s) is the space coordinate. The expression $U_w(s) = ae^{s/L}$ depicts the exponential stretching velocity, while T_∞ is ambient and T_w is the curved surface temperature. Keep in view, the above
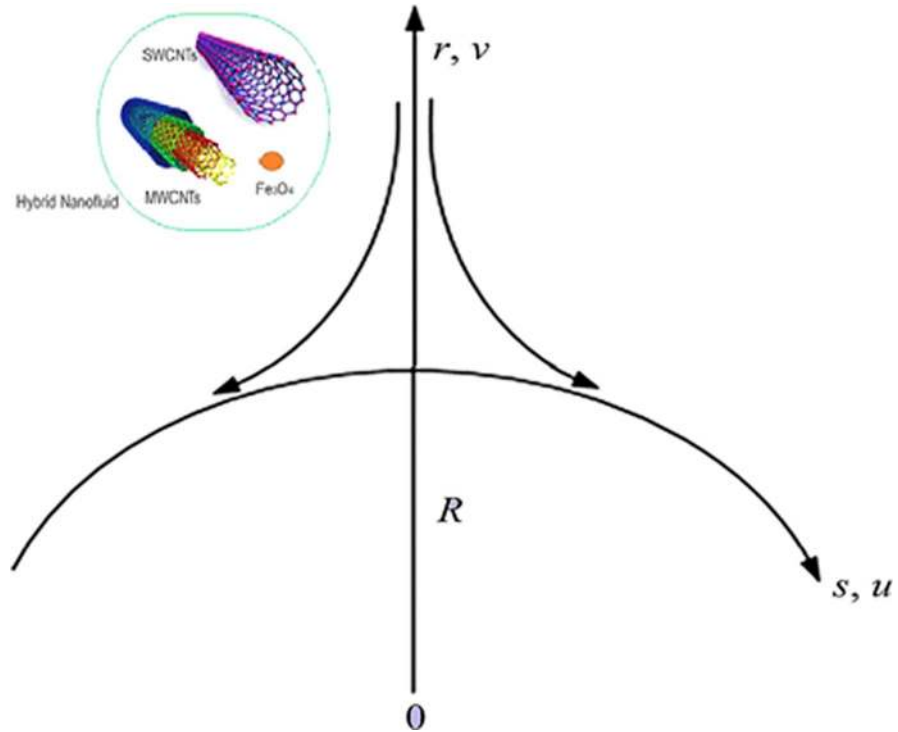
Fig 1.

description of the velocity and energy equation along with their boundary condition is formulated as [37,38]:

$$\frac{\partial}{\partial r}\left((r+u)v\right) + R\frac{\partial u}{\partial r} = 0, \tag{1}$$

$$\frac{u^2}{r+R} = \frac{1}{\rho_{hnf}}\frac{\partial p}{\partial r}, \tag{2}$$

$$v\frac{\partial u}{\partial r} + \frac{R}{r+R}u\frac{\partial u}{\partial s} + \frac{uv}{r+R} = -\frac{1}{\rho_{hnf}}\frac{R}{r+R}\frac{\partial p}{\partial s} +$$
$$v_{hnf}\left(\frac{\partial^2 u}{\partial r^2} + \frac{1}{r+R}\frac{\partial u}{\partial r} - \frac{u}{(r+R)^2}\right) - \frac{v_{hnf}}{K^*}u - Fu^2, \tag{3}$$

$$\left[v\frac{\partial T}{\partial r} + u\frac{\partial T}{\partial s}\frac{R}{r+R}\right] = \alpha_{hnf}\left(\frac{\partial^2 T}{\partial r^2} + \frac{1}{r+R}\frac{\partial T}{\partial r}\right), \tag{4}$$

$$\left[v\frac{\partial C}{\partial r} + u\frac{\partial C}{\partial s}\frac{R}{r+R}\right] = D_{hnf}\left(\frac{\partial^2 C}{\partial r^2} + \frac{1}{r+R}\frac{\partial C}{\partial r}\right). \tag{5}$$

Where u, v represent the component of velocity in s and r-direction. Here, $F = \frac{C_b}{sK^{*1/2}}$, is the non-uniform inertia coefficient and K^* is the porous space permeability.

The basic flow conditions are:

$$v = 0, u = U_w(s) = ae^{s/L}, T = T_\infty + T_0 e^{As/2L} = T_w, C = C_\infty + C_0 e^{As/2L} = C_w, \text{ at } r = 0,$$

$$u \to 0, \frac{\partial u}{\partial r}, T \to T_\infty, C \to C_\infty, \text{ at } r \to \infty$$

(6)

2.1 Expressions for hybrid nanofluid

$$v_{hnf} = \frac{\mu_{hnf}}{\rho_{hnf}}, \mu_{hnf} = \frac{\mu_f}{(1-\phi_1)^{5/2}(1-\phi_2)^{5/2}}, \frac{(\rho)_{hnf}}{(\rho)_f} = (1-\phi_2)\left\{1 - \left(1 - \frac{(\rho)Ms}{(\rho)_f}\right)\phi_1\right\} + \frac{(\rho)_{CNT}}{(\rho)_f}\phi_2,$$

$$\frac{(\rho C_p)_{hnf}}{(\rho C_p)_f} = (1-\phi_2)\left\{1 - \left(1 - \frac{(\rho C_p)Ms}{(\rho C_p)_f}\right)\phi_1\right\} + \frac{(\rho C_p)_{CNT}}{(\rho C_p)_f}\phi_2,$$

(7)

$$\frac{k_{hnf}}{k_{bf}} = \frac{1 - \phi_2 + 2\phi_2 \frac{k_{CNT}}{(k_{CNT} - k_{bf})} - \ln\frac{k_{CNT} + k_{bf}}{2k_{bf}}}{1 - \phi_2 + 2\phi_2 \frac{k_{bf}}{(k_{CNT} - k_{bf})} - \ln\frac{k_{CNT} + k_{bf}}{2k_{bf}}}, \frac{k_{bf}}{k_f} = \frac{k_{MS} + (m-1)_{kf} - (m-1)\phi_1(k_f - k_{MS})}{k_{MS} + (m-1)_{kf} - \phi_1(k_f - k_{MS})},$$

Pr and Sc indicated the Prandtl and Schmidt number. $(C_p)_{MS}, \rho_{MS}$ and ρ_{CNT} specified capacitance and densities of Fe_3O_4 and CNTs respectively. The k_{hnf}, k_f is the thermal conductivity of nanofluids Fe_3O_4 and carrier fluid H_2O. The density of base fluid H_2O, specific heat and viscosity are illustrated via $\rho_f, (\rho_p)_f$ and μ respectively. The volumetric concentration of Fe_3O_4 and carbon nanotubes are denoted by ϕ_1 and ϕ_2.

The appropriate transformation is [37–39]:

$$\eta = \left(\frac{ae^{s/L}}{2v_f L}\right)^{1/2} r, v = -\frac{R}{r+R}\sqrt{\frac{av_f e^{s/L}}{2L}}(f(\eta) + \eta f'(\eta)), u = U_w = ae^{s/L}f'(\eta),$$

$$p = \rho_f a^2 e^{2s/L} H(\eta), T = T_\infty + T_0 e^{\frac{As}{2L}}\Theta(\eta), C = C_\infty + C_0 e^{\frac{As}{2L}}\Phi(\eta).$$

(8)

Utilizing the above similarity transformations, the present governing equations turns into nonlinear coupled ordinary differential equations, which are presented as follows

$$H' = \left(\frac{(\rho)_{hnf}}{(\rho)_f}\right)\frac{1}{\eta + K}f'^2,$$

(9)

$$\left(f''' + \frac{1}{\eta+K}f'' - \frac{1}{(\eta+K)^2}f' - 2\lambda f'\right) - (1-\phi_1)^{2.5}(1-\phi_2)^{2.5}\left(\frac{(\rho)_{hnf}}{(\rho)_f}\right)$$

$$\left(\frac{\eta + 2K}{(\eta+K)^2}K(f')^2 - \frac{K}{\eta+K}ff'' - \frac{K}{(\eta+K)^2} + 2Frf'^2\right) = (1-\phi_1)^{2.5}(1-\phi_2)^{2.5}\frac{K}{\eta+K}(4H + \eta H).$$

(10)

$$\frac{k_{hnf}}{k_f}\left(\Theta'' + \frac{1}{\eta+K}\Theta'\right) + \left(\frac{(\rho C_p)_{hnf}}{(\rho C_p)_f}\right)\Pr\frac{K}{\eta+K}(f\Theta' - Af'\Theta) = 0,$$

(11)

$$(1-\phi_1)(1-\phi_2)\left(\Phi'' + \frac{1}{\eta+K}\Phi'\right) + Sc\left(\frac{K}{\eta+K}f\Phi'\right) = 0.$$

(12)

By eliminating H from Eqs ([9]) and ([10]), we get

$$
\left[f^{iv} + \frac{2}{\eta + K} f''' - \frac{1}{(\eta + K)^2} f'' + \frac{1}{(\eta + K)^3} f' - 2\lambda \left(f'' + \frac{1}{(\eta + K)} f' \right) \right] +
$$
$$
\frac{(\rho)_{hnf}}{(\rho)_f} \left[\begin{array}{l} \dfrac{K}{(\eta + K)^2} ff'' + \dfrac{K}{(\eta + K)} ff''' - \dfrac{K}{(\eta + K)^3} ff' \dfrac{3K}{(\eta + K)^2 f'^2} - \dfrac{3K}{(\eta + K)} f'f'' \\ \\ -2Fr\left(2f'f'' + \dfrac{1}{\eta + K} f'^2 \right) \end{array} \right] = 0,
\tag{13}
$$

The transform conditions for nonlinear differential equations are:

$$
f = 0, f' = 1, \Theta = 1, \Phi = 1, \text{ at } \eta = 0.
$$
$$
f' \to 0, f'' \to 0, \Theta \to 0, \Phi \to 0, \text{ at } \eta = \infty.
\tag{14}
$$

In the above transform equation Fr depicts Forchheimer number, Pr is the Prandtl number, K is the Curvature parameter, λ is the local porosity parameter and Schmidt number are defined as:

$$
Fr = \frac{C_b}{K^{*1/2}}, \Pr = \frac{\upsilon_f}{\alpha_f}, K = \left(\frac{ae^{s/L}}{2\upsilon_f L} \right), \lambda = \frac{\upsilon_f L}{K^* U_w}, Sc = \frac{\upsilon_f}{D_f}.
\tag{15}
$$

2.2 Quantities of physical interest

The expression for the local Nusselt number, Sherwood Number and Skin friction are given as

$$
\frac{L}{S} \left(\frac{\text{Re}}{2} \right)^{\frac{-1}{2}} Nu_x = -\frac{k_{hnf}}{k_{bf}} \Theta'(0), \quad \frac{L}{S} \left(\frac{\text{Re}}{2} \right)^{\frac{-1}{2}} Sh_x = -\Phi'(0),
$$
$$
\sqrt{\frac{\text{Re}}{2}} C_{fx} = \frac{1}{(1 - \phi_1)^{2.5} (1 - \phi_2)^{2.5}} f''(0).
\tag{16}
$$

Where local Reynolds number is

$$
\text{Re}_x = \frac{u_0 x^2}{\nu l}.
\tag{17}
$$

3. Problem solution

The problem is solved through the HAM technique, which was offered by Liao [40–42]. The initial approximation for velocity f_0 and temperature Θ_0 are given a

$$
f_0(\eta) = e^{-\eta} - e^{-2\eta}, \Theta_0(\eta) = e^{-\eta}, \ \Phi_0(\eta) = e^{-\eta}.
\tag{18}
$$

The linear operatives are offered as:

$$
\mathscr{L}_f(\mathrm{f}) = f^{iv} \ \text{ and } \ \mathscr{L}_\Theta(\Theta) = \Theta''.
\tag{19}
$$

The expand form of $\mathscr{L}_f$, $\mathscr{L}_\Theta$ and $\mathscr{L}_\Phi$ are:

$$
\mathscr{L}_f[\chi_1 + \chi_2 \eta + \chi_3 \eta^2 + \chi_4 \eta^3] = 0, \ \ \mathscr{L}_\Theta[\chi_5 + \chi_6 \eta] = 0, \ \ \mathscr{L}_\Phi[\chi_7 + \chi_8 \eta] = 0.
\tag{20}
$$

3.1 OHAM convergence

The convergence of the OHAM method has been obtained using the idea of Liao [40,42].

$$\varepsilon_m^f = \frac{1}{l+1} \sum_{j=1}^{l} \left[N_f \left(\sum_{k=1}^{m} f(\eta) \right)_{\eta=j\delta\eta} \right]^2, \tag{21}$$

$$\varepsilon_m^\Theta = \frac{1}{l+1} \sum_{j=1}^{l} \left[N_\Theta \left(\sum_{k=1}^{m} f(\eta), \sum_{k=1}^{,m} \Theta(\eta), \right)_{\eta=j\delta\eta} \right]^2, \tag{22}$$

$$\varepsilon_m^\Phi = \frac{1}{l+1} \sum_{j=1}^{l} \left[N_\Phi \left(\sum_{k=1}^{m} \Phi(\eta) \right)_{\eta=j\delta\eta} \right]^2, \tag{23}$$

The whole sum of the square residual is clear as $\varepsilon_m^t = \varepsilon_m^f + \varepsilon_m^\Theta + \varepsilon_m^\Phi$.

4. Results and discussion

This section aims to visualize variations in temperature, flow, Nusselt number, and skin friction coefficient for involved parameters like Fr depicts Forchheimer number, Pr is the Prandtl number, K is the Curvature parameter, λ is the local porosity parameter and Schmidt number. Fig 1 exhibits the geometry of the flow problem. The OHAM method's convergence has been calculated up to the 30th order estimation and shown in Fig 2. Comparative investigation of nanofluid (Fe_3O_4+ H_2O) and hybrid nanofluid (MWCNTs + Fe_3O_4 + H_2O) and (SWCNTs + Fe_3O_4 + H_2O) during studying impacts of λ, Fr, K and ϕ_1, ϕ_2 on $f(\eta)$ is visualized in Figs 3–6, respectively. Efficient trend is shown by hybrid

Fig 2.

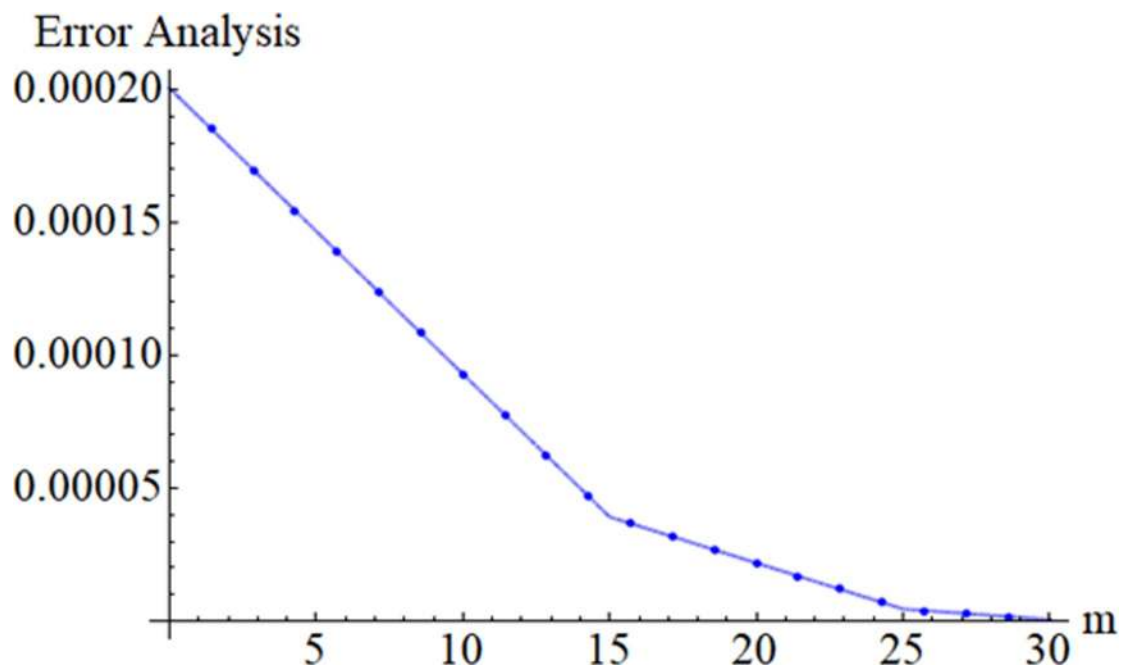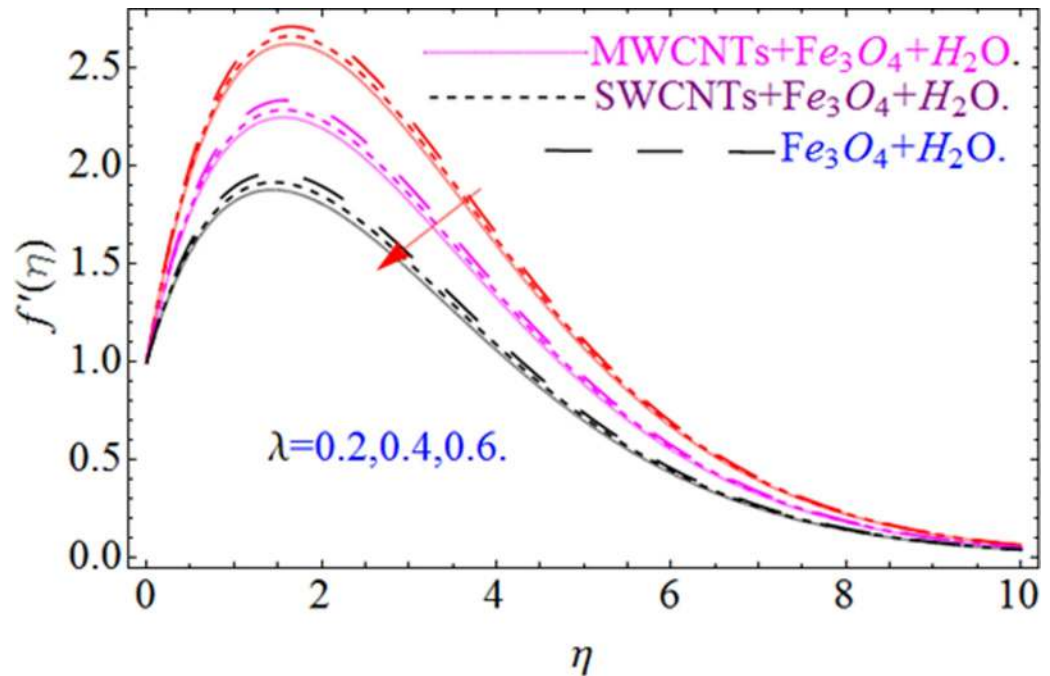https://doi.org/10.1371/journal.pone.0249434.g002

Fig 3.

nanomaterial (MWCNTs + Fe_3O_4 + H_2O) which is followed by (SWCNTs + Fe_3O_4 + H_2O) and (Fe_3O_4+ H_2O). The velocity profile ($f'(\eta)$) under higher estimations of λ (local porosity parameter) is sketched in Fig 3. Higher estimation of λ (local porosity parameter) leads to decay of $f'(\eta)$. Physically, λ is inversely proportional to darcian drag force which implies the Darcy number reduces the rise of darcian drag force, hence this is acts to enhance the permeability of the fluid flow and it leads to diminishes the fluid velocity. Enhancement of permeability rises to the resistive force within the particles so that the fluid's velocity will be reduced. It is noted that the velocity of nanofluid (Fe_3O_4+ H_2O) rapidly decreases as compared to hybrid nanofluid (MWCNTs + Fe_3O_4 + H_2O) and (SWCNTs + Fe_3O_4 + H_2O). Fig 4 is sketched to demonstrate the effect of ϕ_1 and ϕ_2 on $f'(\eta)$. Higher estimation of ϕ_1 and ϕ_2 leads to decrement of $f'(\eta)$. The transportation, cohesive forces, and excitation energy between carbon nanotubes nanoliquid and iron oxide nanoliquid decreases by increasing the quantity of volume fraction, which causes negative changes in the velocity field $f'(\eta)$. The iron oxide Fe_3O_4 nanoliquid show greater velocity as compared to multi and single- wall carbon nanotubes, because metal atoms have free valence electrons in the valence shell than CNTs and exert a weaker force on it. Fig 5 visualizes impacts of k (curvature parameter) on velocity field $f'(\eta)$ for nanofluid (Fe_3O_4 + H_2O) and hybrid nanofluid (MWCNTs + Fe_3O_4 + H_2O) and (SWCNTs + Fe_3O_4 + H_2O). Intensification in the velocity of fluid $f'(\eta)$ is examined via higher estimations of k. Physically, with the growing credit of k the radius R of the stretching surface increases, which improves the fluid velocity of both CNTs nanoliquid and Fe_3O_4 nanoliquid. Furthermore, the impacts of nanofluid (Fe_3O_4 + H_2O) dominate when compared with nanomaterial hybrid nanofluid (MWCNTs + Fe_3O_4 + H_2O) and (SWCNTs + Fe_3O_4 + H_2O). Velocity profile $f'(\eta)$ for variations in Fr is portrayed in Fig 6 for nanofluid (Fe_3O_4 + H_2O) and hybrid nanofluid (MWCNTs + Fe_3O_4 + H_2O) and (SWCNTs + Fe_3O_4 + H_2O). Higher Fr leads to enlargement of $f'(\eta)$.
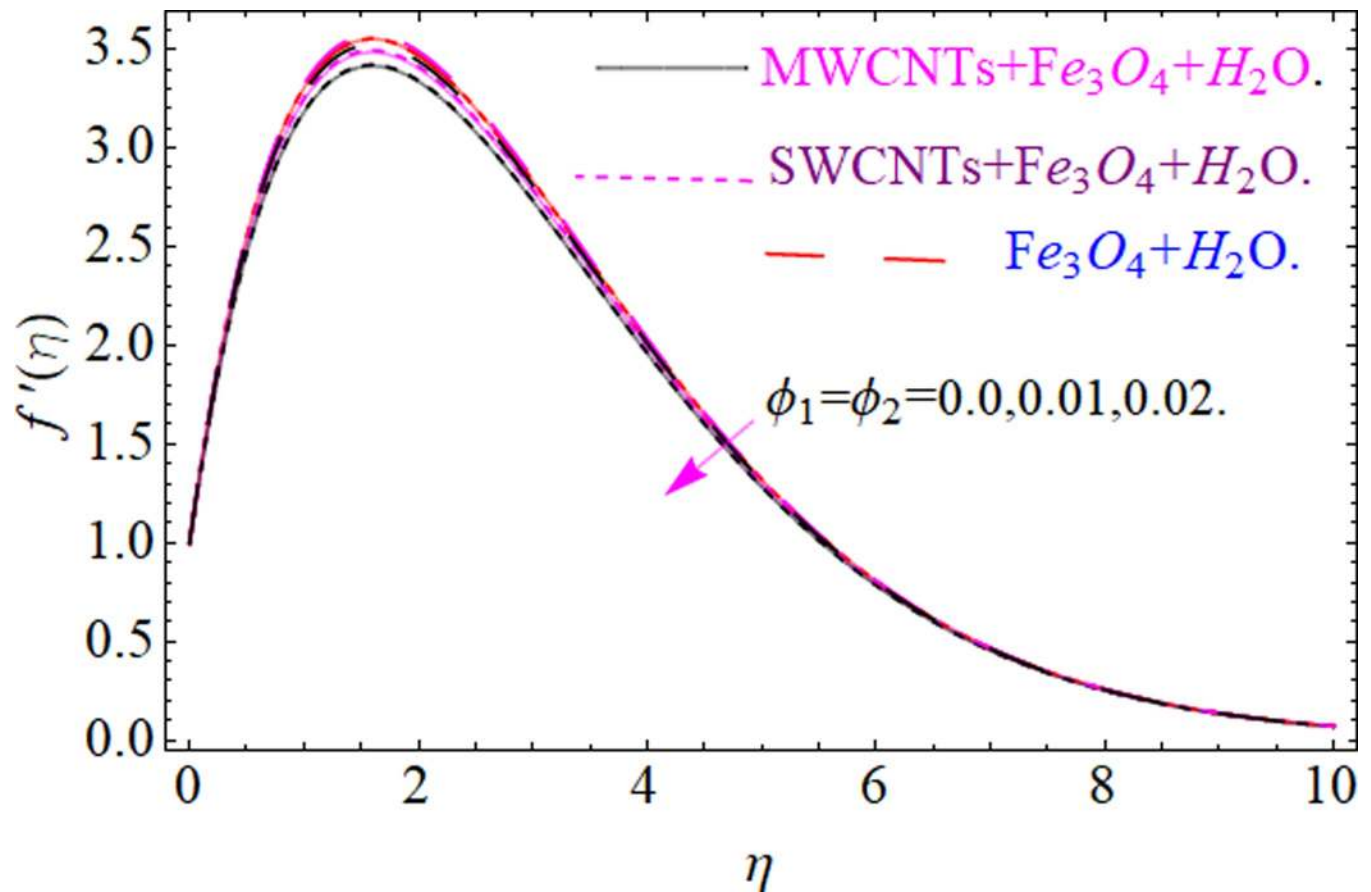
Fig 4.

Physically, this mechanism happens due to the inertial effect that drags the fluid backward and accordingly with this inertial force, the speed of fluid will be decreased; therefore, the velocity profile is declined. Moreover, the impacts of hybrid nanofluid (SWCNTs + Fe_3O_4 + H_2O) dominate when compared with nanomaterial hybrid nanofluid (MWCNTs + Fe_3O_4 + H_2O) and nanofluid (Fe_3O_4 + H_2O). Comparative investigations amongst hybrid nanomaterial (MWCNTs + Fe_3O_4 + H_2O) and (SWCNTs + Fe_3O_4 + H_2O) and nanomaterial (Fe_3O_4 + H_2O) via impacts of k, λ, Fr, A and ϕ_1, ϕ_2 on temperature profile $\Theta(\eta)$ are visualized in Figs 7–11, respectively. Fig 7 depicts the k (curvature parameter) influence on the temperature $\Theta(\eta)$ profile for nanofluid (Fe_3O_4 + H_2O) and hybrid nanofluid (MWCNTs + Fe_3O_4 + H_2O) and (SWCNTs + Fe_3O_4 + H_2O). As the curvature parameter increases, the radius of the stretching surface also increases, which ensure that the maximum number of nanoparticles will be attached to the stretching surface, which will conduct more heat, as a result, the temperature field of CNTs nanoliquid and Fe_3O_4 nanoliquid enhances. While opposite behavior has been observed with the increment of the Forchhemier number Fr in Fig 8. It is characterized that the improvement of Fr declines the temperature field $\Theta(\eta)$. Furthermore such reduction in temperature of nanofluid (Fe_3O_4 + H_2O) is more quickly as compared to hybrid nanofluids (MWCNTs + Fe_3O_4 + H_2O) and (SWCNTs + Fe_3O_4 + H_2O). Fig 9 is drawn to characterize the impact of ϕ_1 and ϕ_2 (volume fraction of CNTs and iron oxide nanoparticles respectively) on heat
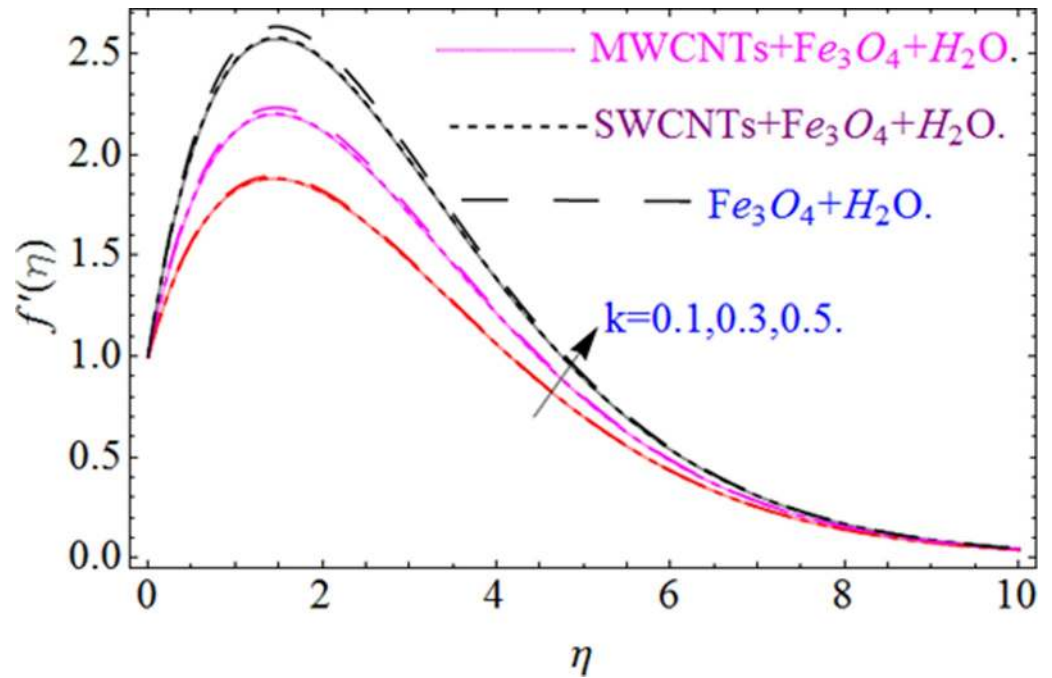
Fig 5.

transfer $\Theta(\eta)$ for hybrid nanomaterial (MWCNTs + Fe_3O_4 + H$_2$O) and (SWCNTs + Fe_3O_4 + H$_2$O) and nanomaterial (Fe_3O_4 + H$_2$O). It is found that the temperature profile boost
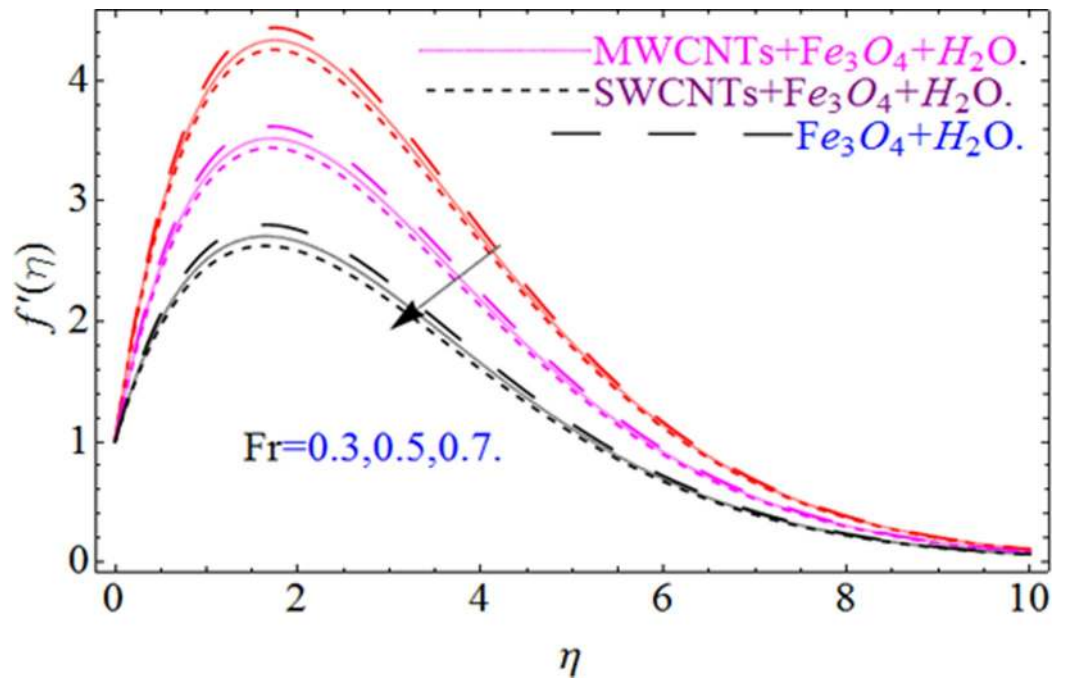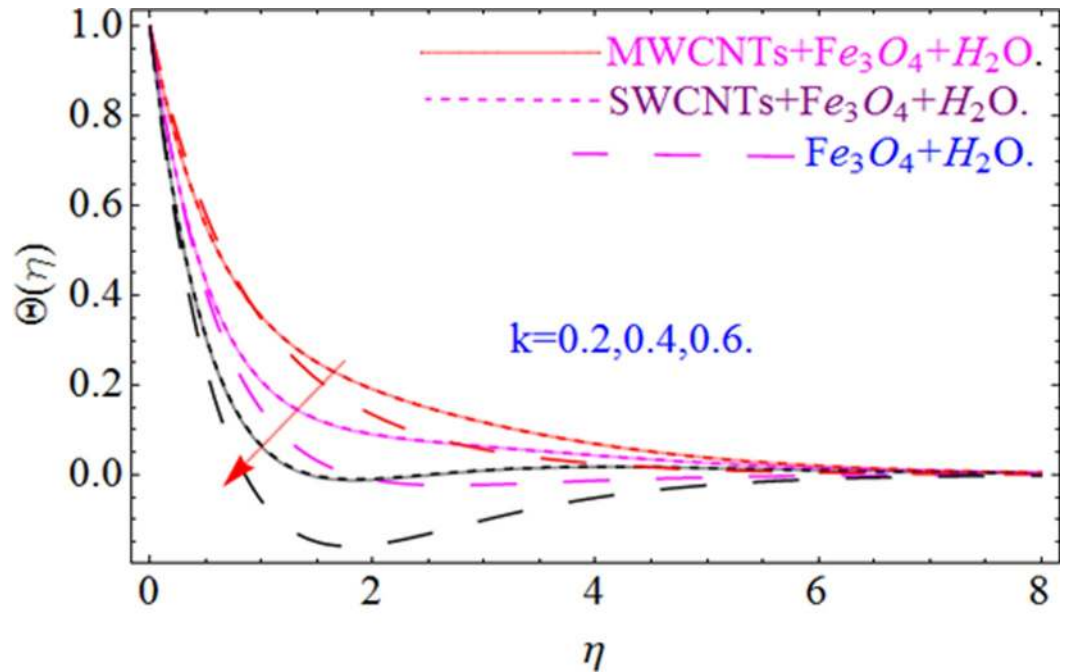

Fig 6.

Fig 7.

with the growing values of ϕ_1 and ϕ_2 for both types of nanofluids. Also the reducing trend has been observed with larger values of A (temperature exponent) in the temperature field
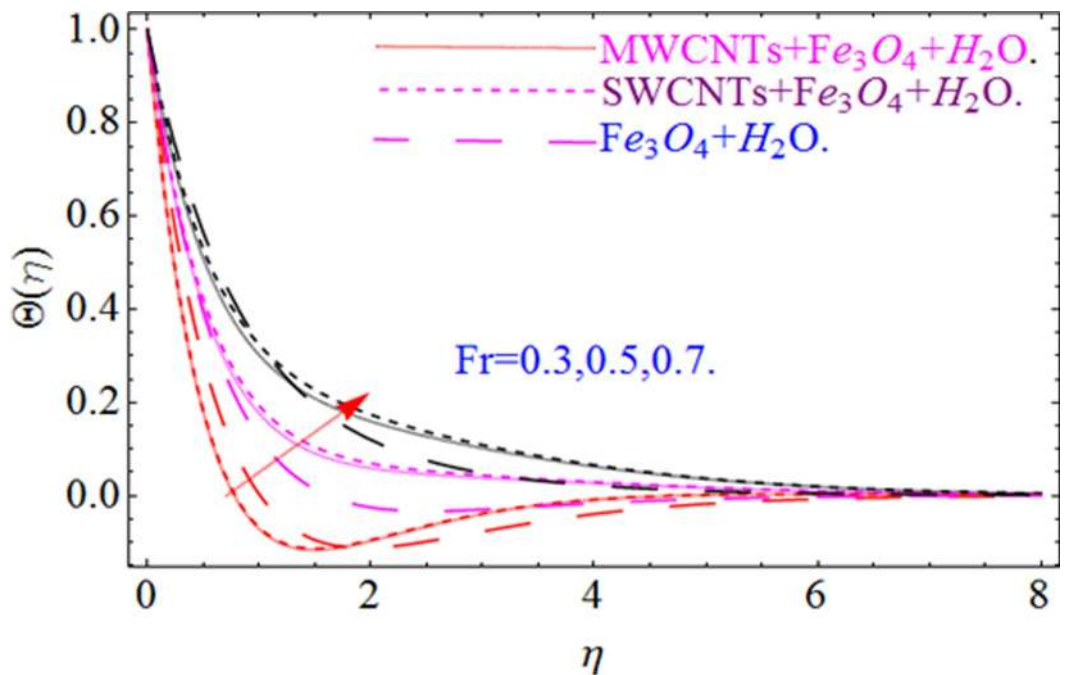

Fig 8.

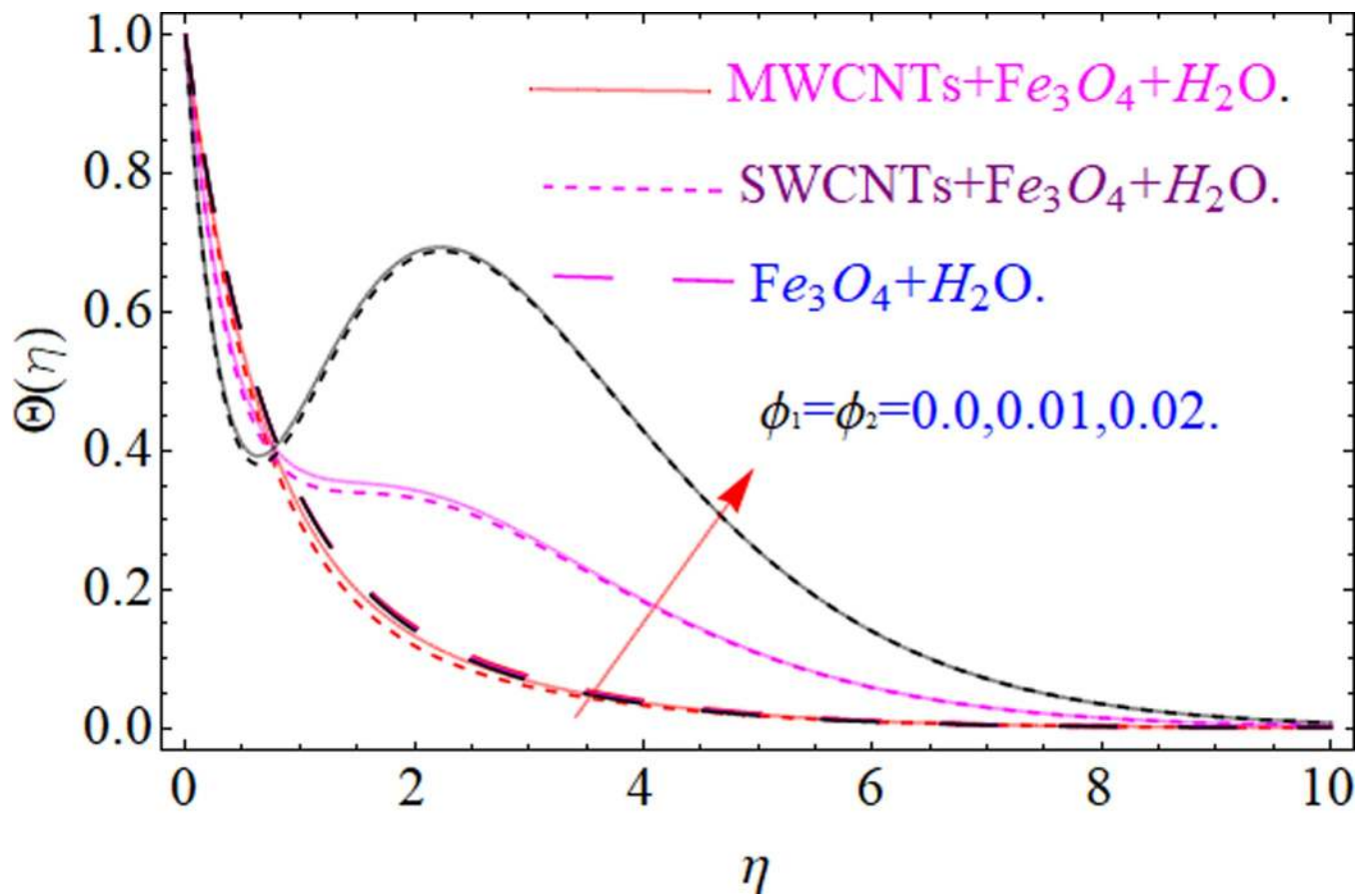**Fig 9.**

Fig 10.

Fig 11.
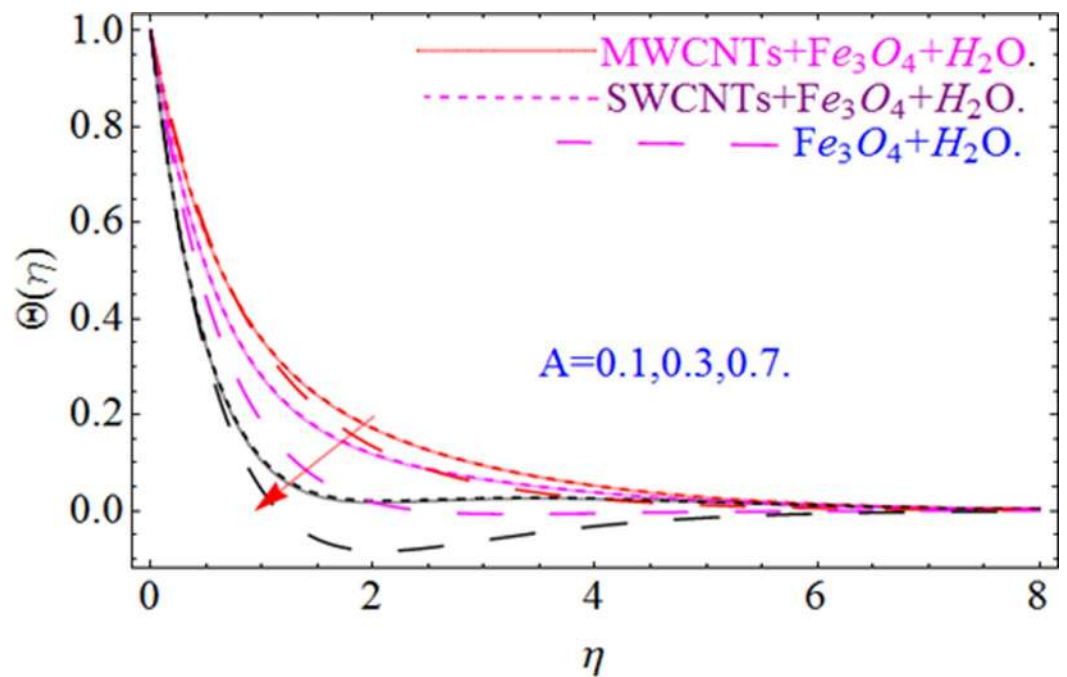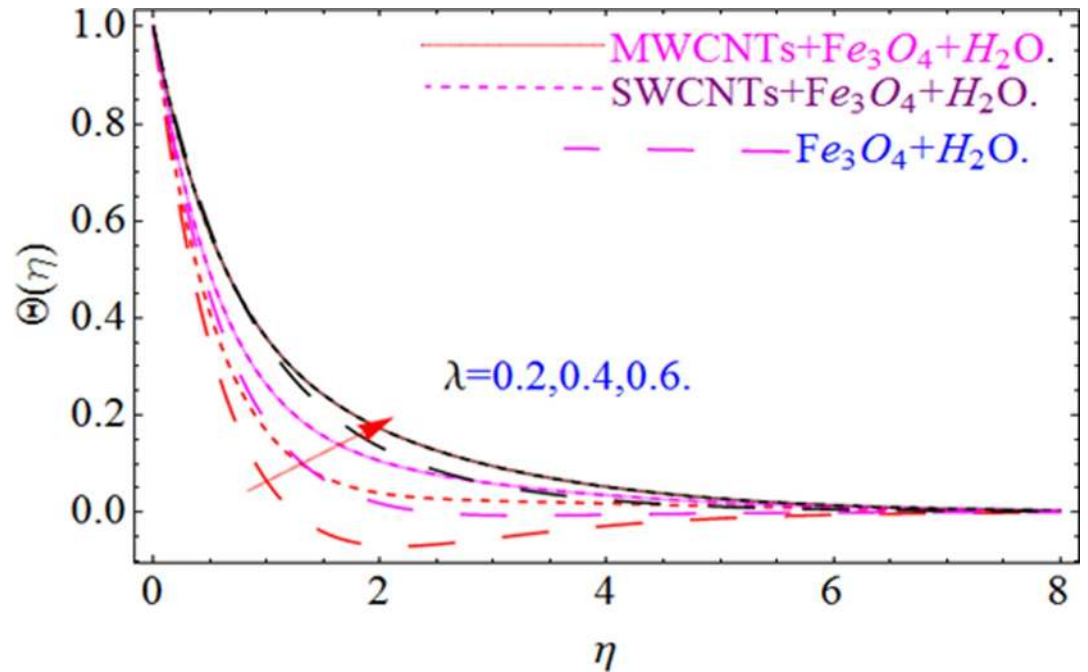
$\Theta(\eta)$ captured in Fig 10. This increment in the temperature profile is more rapidly in case of nanofluid (Fe_3O_4 + H_2O) as equated to hybrid nanofluids (MWCNTs + Fe_3O_4 + H_2O)
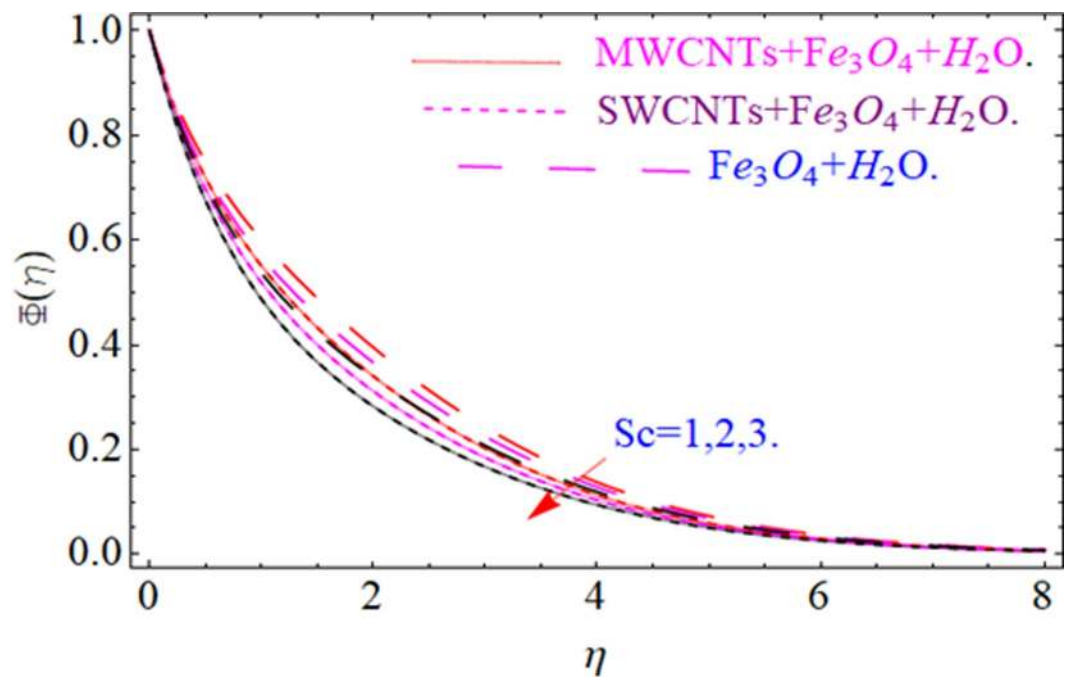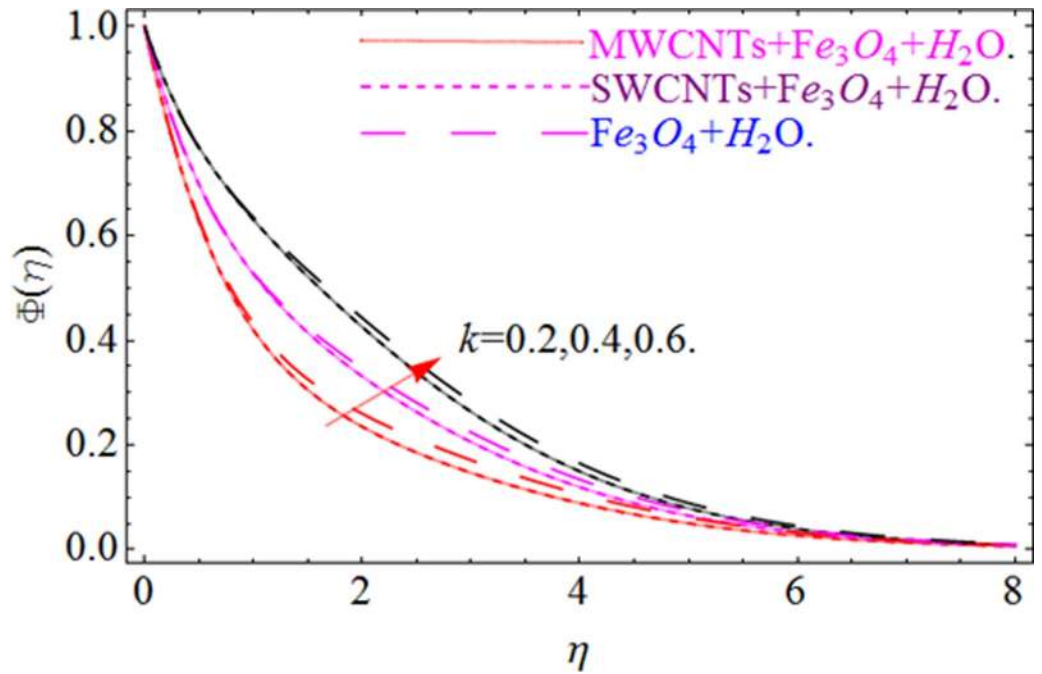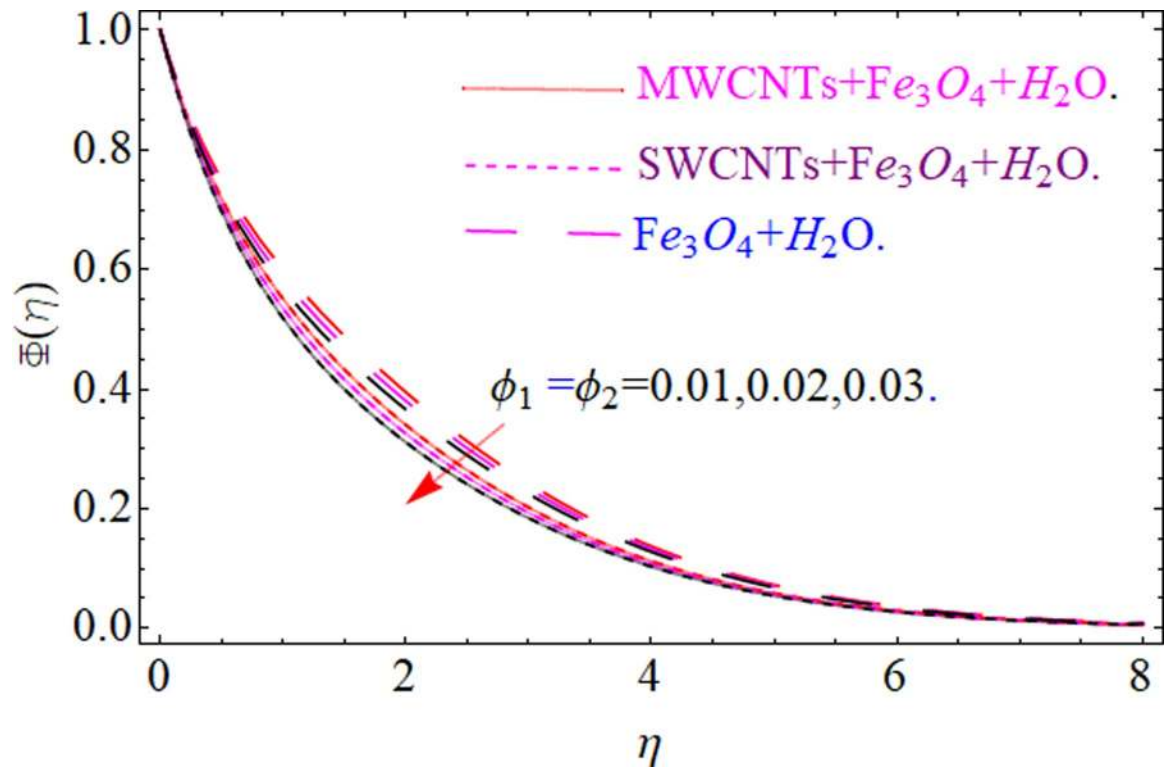

Fig 12.

Fig 13.

https://doi.org/10.1371/journal.pone.0249434.g013

Fig 14.

https://doi.org/10.1371/journal.pone.0249434.g014
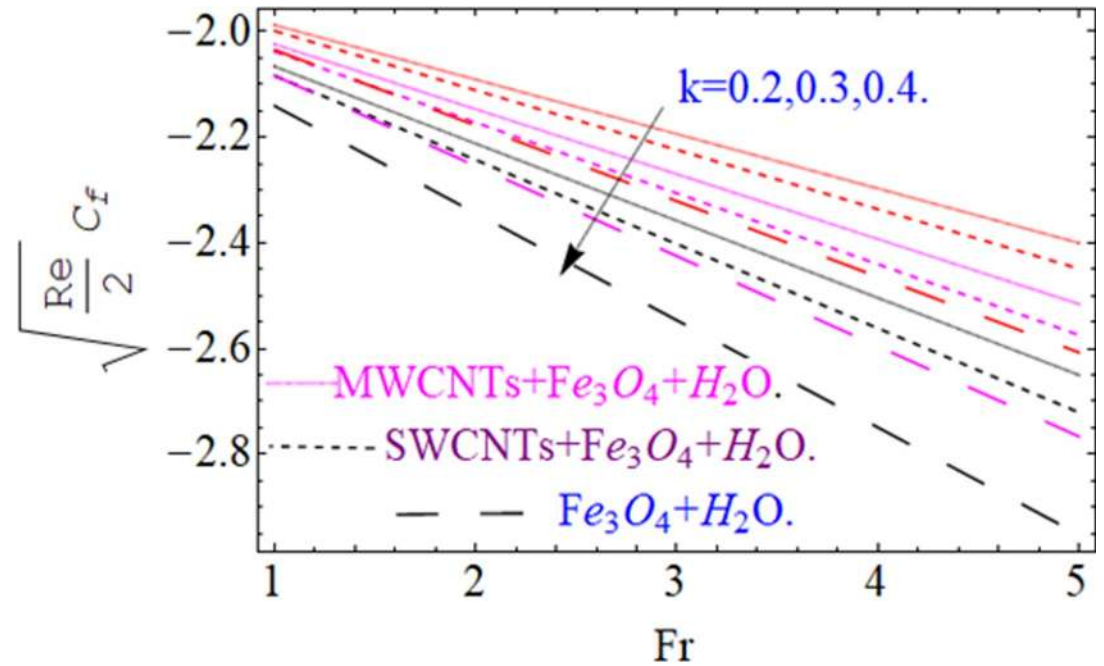
Fig 15.

Fig 16.

Fig 17.

Fig 18.

Table 1. The Thermophysical properties of CNTs, Fe$_3$O$_4$ and base fluid water [19,29].

Thermophysical properties	ρ(kg/m^3)	C_p(j/kgK)	k(W/mK)
SWCNTs	2600	425	6600
MWCNTs	1600	796	300
Fe$_3$O$_4$	5200	670	6
Pure water	997.1	4179	0.613

and (SWCNTs + Fe_3O_4 + H$_2$O). Fig 11 visualizes the impacts of porosity parameter λ on temperature field $\Theta(\eta)$ for hybrid nanomaterial (MWCNTs + Fe_3O_4 + H$_2$O) and (SWCNTs + Fe_3O_4 + H$_2$O) and nanomaterial (Fe_3O_4 + H$_2$O). Intensification in temperature field $\Theta(\eta)$ is examined via higher estimations of λ. Similarly, Comparative investigations amongst hybrid nanomaterial (MWCNTs + Fe_3O_4 + H$_2$O) and (SWCNTs + Fe_3O_4 + H$_2$O) and nanomaterial (Fe_3O_4 + H$_2$O) via impacts of k, λ, Fr, A and ϕ_1, ϕ_2 on concentration profile $\Phi(\eta)$ are visualized in Figs 12–14, respectively. The impact of Schmidt number Sc and curvature parameter k on mass transfer $\Phi(\eta)$ are presented in Figs 12 and 13 for hybrid nanomaterial (MWCNTs + Fe_3O_4 + H$_2$O) and (SWCNTs + Fe_3O_4 + H$_2$O) and nanomaterial (Fe_3O_4 + H$_2$O), respectively. The associated boundary layer thickness and concentration, increases with Schmidt numbe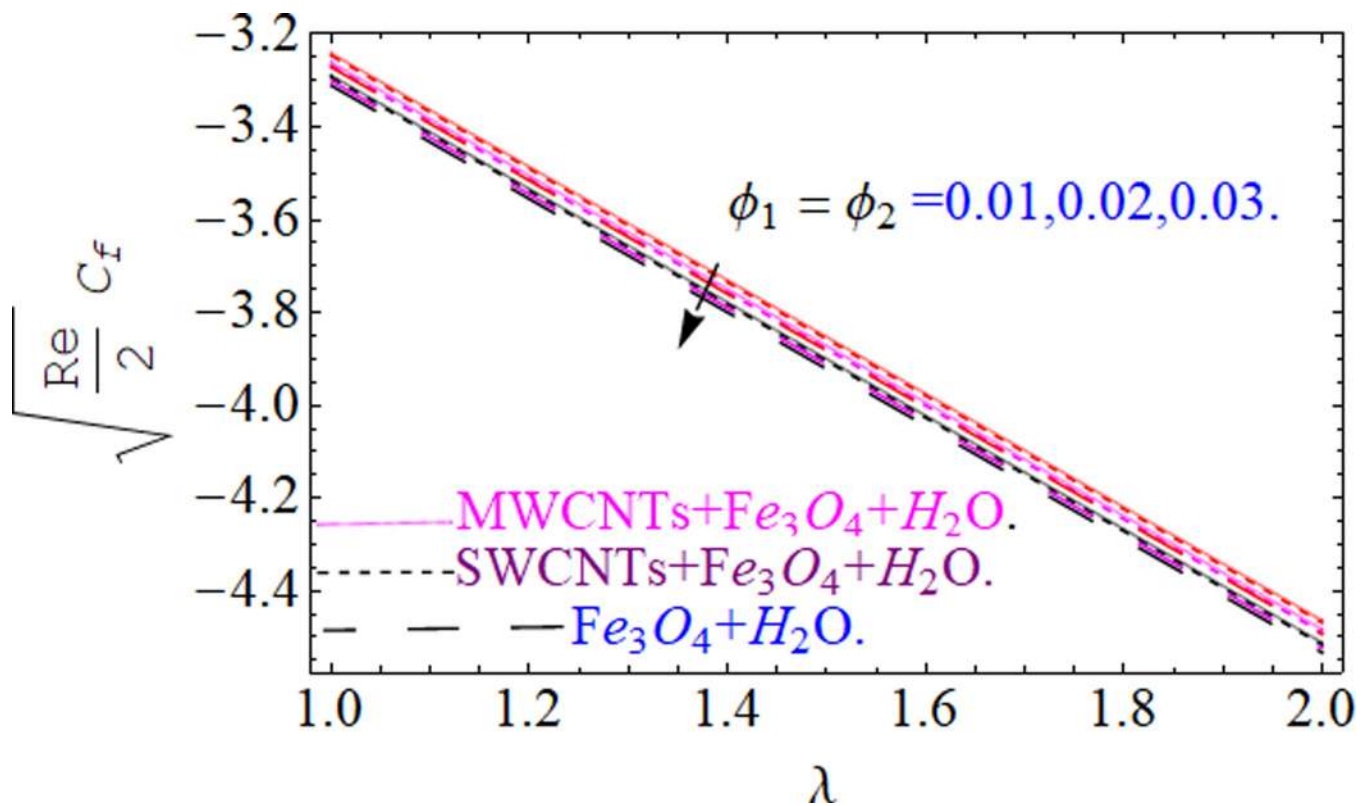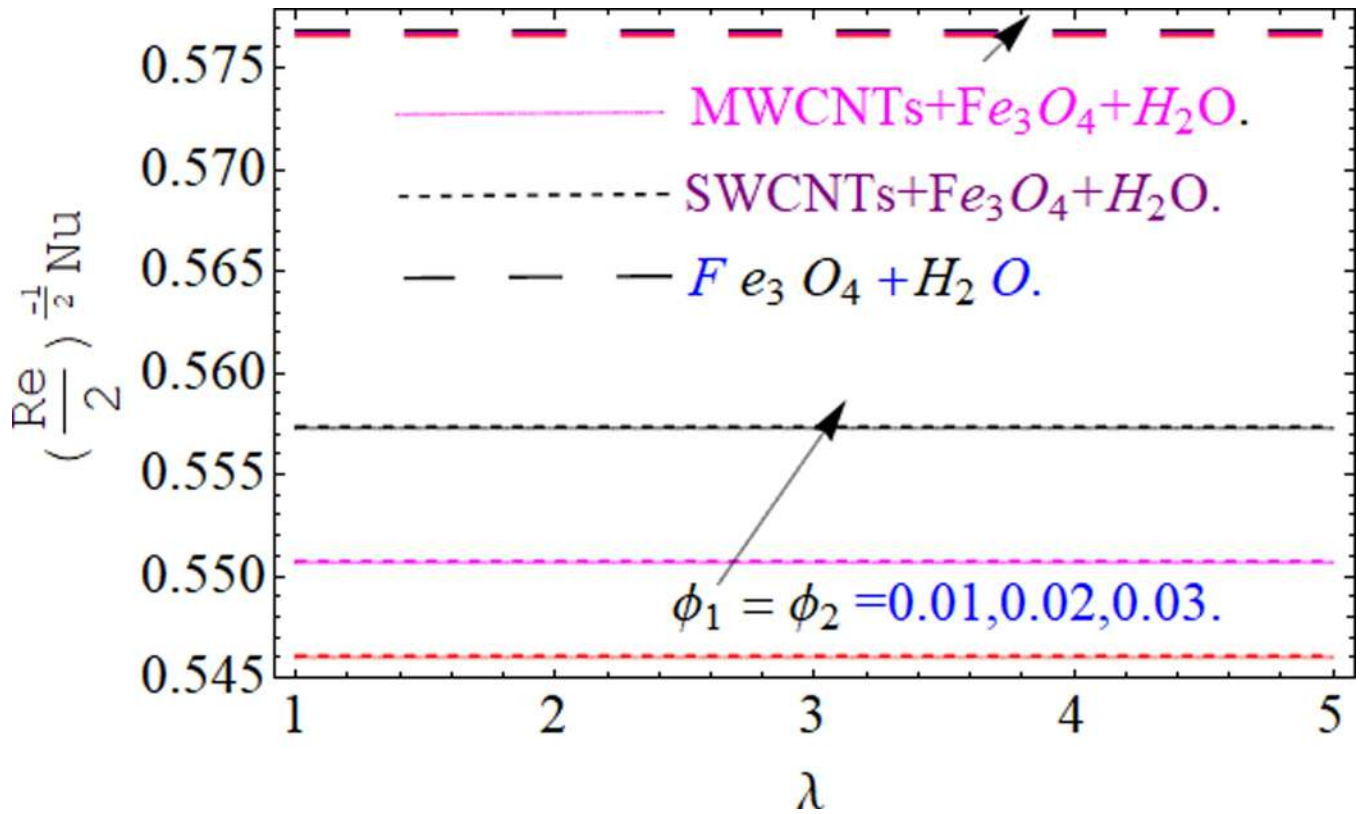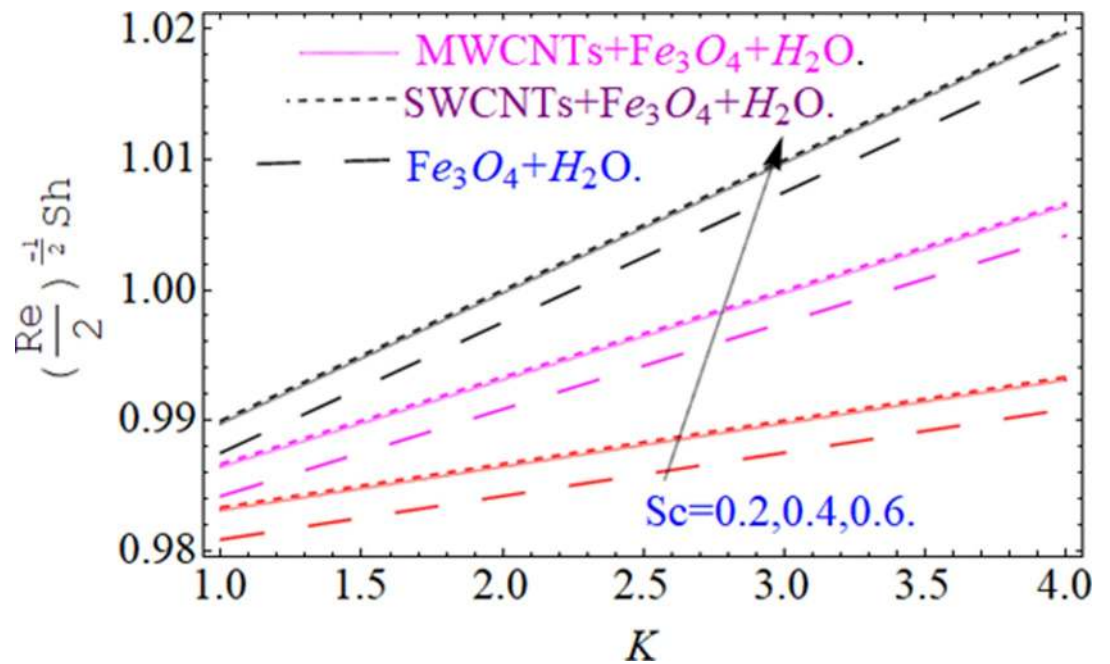r Sc, while opposite behavior has been examined in Fig 13. Because the mass transfer rate diminishes with increases of curvature factor k. Fig 14 demonstrate the influence of volume fraction indicator ϕ_1 and ϕ_2 for both CNTs and ferrium oxide nanoliquid on concentration profile $\Phi(\eta)$. The improvement in quantity of iron oxide nanoparticles and carbon nanotubes actually slows down the mass transfer rate, because the fluid average viscosity becomes dense. Thus the concentration profile decline with growing credit of ϕ_1 and ϕ_2. The surface drag force $\sqrt{\frac{Re}{2}}C_{fx}$ for carbon nanoliquid and Fe_3O_4 are declared via Figs 15 and 16. It is perceived that the skin friction reduces with the positive increment of curvature factor k and volume friction parameter ϕ_2. Fig 17 illustrate the numerical outcomes for Nusselt number $\frac{L}{S}\left(\frac{Re}{2}\right)^{\frac{-1}{2}}Nu_x$. It is examined that the heat transmission rate improved with the improvement of the carbon nanotubes ϕ_2 quantity in base fluid. The Sherwood number $\frac{L}{S}\left(\frac{Re}{2}\right)^{\frac{-1}{2}}Sh_x$ is the improving function of the Schmidt number shown in Fig 18.

The thermo physical properties of the solid materials and base fluids are shown in the Table 1. The OHAM method's convergence has been calculated up to the 30th iteration and displayed in Table 2. The comparison of the present work with the available literature is revealed in Table.3. In Table 4, the enhancement in heat transfer rate for the SWCNTs, MWCNTs and Iron Oxide water based nanofluids have been calculated in %. According to the obtained results,

Table 2. The total residual errors.

m	$\varepsilon_m^t SWCNTs$	$\varepsilon_m^t SWCNTs$	$\varepsilon_m^t Fe_3O_4$
5	1.8168×10^{-4}	1.9479×10^{-4}	1.4257×10^{-4}
13	1.1223×10^{-5}	1.2354×10^{-5}	1.18312×10^{-5}
23	1.3599×10^{-6}	0.4698×10^{-6}	0.4489×10^{-6}
30	3.2578×10^{-7}	4.3689×10^{-7}	4.1464×10^{-7}

When $Fr = k = 0.6$, $\phi_1 = 0.02$, $\phi_2 = 0.2$, $\lambda = 0.2$, $Pr = 6.3$, $A = 0.4$.

Table 3. Present study and Hayat et al. [36].

	Hayat et al. [35]	Present
$f''(0)$	0.735	0.7352130
$-\Theta'(0)$	-1.375	-1.3752410
$-\Phi'(0)$	. . . .	-1.3620189

When $\phi_1 = \phi_2 = \phi = 0$, $Fr = k = 0.6$, $\lambda = 0.2$, Pr = 6.3, A = 0.4.

https://doi.org/10.1371/journal.pone.0249434.t003

iron oxide nanoparticles are more efficient in enhancing the heat transfer rate. Similarly, the SWCNTs are comparatively more reliable for the heat transfer rate as compared to MWCNTs.

5. Conclusion

In the existing study, we talked about the Darcy Forchheimer flow of hybrid nanoliquid due to an extending curved surface. The flow model is arranged in the form of differential equations containing momentum and energy equation. The analytic arrangement of modeled equations is further set up by the "Homotopy analysis method" (HAM). The concluded findings are pointed out as:

- The temperature and velocity fields, both show similar behaviors for rising values of volume fraction parameters of CNTs and Fe_3O_4.

- To keep maintain the coolant level in the industrial equipment's uses of CNT and Fe_3O_4 nanoparticles is significantly useful.

- The reducing trend has been observed in temperature with larger values of A (temperature exponent).

- The improving credit of k (curvature parameter) results in high fluid velocity, while reducing the temperature of the fluid.

- But Forchheimer number shows the opposite trend for temperature and velocity profile, because with increases of Fr the fluid velocity reduces, while the temperature profile enhances.

- The % increase in the heat transfer rate observed using the hybrid nanofluid. It is perceived that the hybrid nanofluid enhance the heat transfer rate (3.1461%) as compared to the other traditional fluids.

- The conclusion states that the hybrid nanofluids are the fast agents for the heat transfer analysis as compared to the common fluids.

Table 4. The heat transfer has been calculated percent wise as for the various nanoparticles Pr = 6.2, λ = 0.02, A = 0.2, Fr = 0.3, using the % formula
% Increase $= \frac{\text{With Nanoparticle}}{\text{Without Nanoparticle}} \times 100 =$ Result Result $- 100\% = $ %enhancment.

$\phi_1 = \phi_2$	$\Theta'(0)$ MWCNTs	$\Theta'(0)$ SWCNTs	$\Theta'(0)$ Fe_3O_4
0.0	1.1593	1.1482	1.1535765
0.01	1.1737999 (1.2507% Increase)	1.1636898 (1.3490% Increase)	1.559517 (2.11% Increase)
0.02	1.1849894 (2.215% Increase)	1.1732025 (2.1775% Increase)	1.1898694 (3.1461% Increase)

https://doi.org/10.1371/journal.pone.0249434.t004

Nomenclature	
u, v	Velocity component
r, s	Space coordinates
A	Temperature exponent
k_f	Thermal conductivity of base fluid
a_f	Base fluid thermal diffusivity
μ_f	Dynamic viscosity
v_f	Kinematic viscosity
F	Nonporous inertia parameter
H	Dimensionless pressure
λ	Local porosity parameter
T_w	Wall temperature
Fr	Forchheimer numbers
K	Curvature parameter
Θ	Dimensionless temperature
ϕ	Volume friction
C_f	Skin friction Coefficient
C_b	Drag coefficient
v_{hnf}	Nanofluids kinematic viscosity
μ_{hnf}	Dynamic viscosity of nanofluids
ρ_{hnf}	Nanofluids density
Nu_s	Local Nusselt number
Re_s	Local Reynold number
K^*	Porous media

Supporting information

S1 Data.
(ZIP)

Author Contributions

Formal analysis: Taza Gul, Wiyada Kumam.

Funding acquisition: Poom Kumam.

Investigation: Anwar Saeed.

Methodology: Safyan Mukhtar, Syed Imad Ali Shah, Saleem Nasir.

Software: Safyan Mukhtar, Taza Gul, Saleem Nasir.

Writing – original draft: Anwar Saeed, Wajdi Alghamdi, Syed Imad Ali Shah.

Writing – review & editing: Wajdi Alghamdi, Poom Kumam, Taza Gul, Wiyada Kumam.

References

1. Crane L. J., Flow past a stretching plate, J. Appl. Math. Phy. (ZAMP), 21 (1970), 645–647.

2. Turkyilmazoglu M. Flow of a micropolar fluid due to a porous stretching sheet and heat transfer, Int. J. Nonlinear Mech. 83 (2016), 59–64.

3. Sajid M., Ali N., Javed T. and Abbas Z., Stretching a curved surface in a viscous fluid, Chin. Phys. Lett. 27 (2010), 024703.

4. Imtiaz M., Hayat T., Alsaedi A. and Hobiny A., Homogeneous-heterogeneous reactions in MHD Flow due to unsteady curved stretching surface, J.Mol. Liq. 221 (2016), 245−253.

5. Rosca N. C. and Pop I., Unsteady boundary layer flow over a permeable curved stretching/ shrinking surface, Europ. J. Mech. B/Fluid. 51 (2015), 61–67.

6. Hayat T., Saif R.S., Ellahi R., Muhammad T., Ahmad B., Numerical study for Darcy-Forchheimer Flow due to a curved stretching surface with Cattaneo-Christov heat flux and homogeneous-heterogeneous reactions, Results in Physics. 7 (2017), 2886–2892.

7. Kumar K.A., Sugunamma V., & Sandeep N., Effect of thermal radiation on MHD Casson fluid flow over an exponentially stretching curved sheet, Journal of Thermal Analysis and Calorimetry, 140 (2020), 2377–2385.

8. Imtiaz M., Hayat T., Alsaedi A., Convective Flow of ferrofluid due to a curved stretching surface with homogeneous-heterogeneous reactions. Powder Technology. 310 (2017), 154–162. https://doi.org/10.1016/j.powtec.2017.01.029

9. Imtiaz M., Hayat T., Alsaedi A., & Hobiny A., Homogeneous-heterogeneous reactions in MHD Flow due to an unsteady curved stretching surface, J. of Molec. Liquids, 221(2016), 245–253. https://doi.org/10.1016/j.molliq.2016.05.060

10. Sanni K. M., Asghar S., Jalil M., & Okechi N.F., Flow of viscous fluid along a nonlinearly stretching curved surface, Results in Physics, 7 (2017), 1–4.

11. Khan U., Alkanhal T.A., Ahmed N., Khan I., & Mohyud-Din S.T., Stimulations of Thermophysical Characteristics of Nano-Diamond and Silver Nanoparticles for Nonlinear Radiative Curved Surface Flow. IEEE Access, 7 (2019), 55509–55517.

12. Kempannagari A. K., Buruju R. R., Naramgari S., & Vangala S. Effect of Joule heating on MHD non-Newtonian fluid flow past an exponentially stretching curved surface. Heat Transfer, 49(2020), 3575–3592.

13. Kumar K. A., Sugunamma V., Sandeep N., & Sivaiah S. Physical aspects on MHD micropolar fluid flow past an exponentially stretching curved surface. In Defect and Diffusion Forum, Trans Tech Publications Ltd., 4(2020), 79–91.

14. Kumar K. A., Sugunamma V., Sandeep N., & Reddy J. R. Numerical examination of MHD nonlinear radiative slip motion of non-newtonian fluid across a stretching sheet in the presence of a porous medium. Heat Transfer Research, 50(2019).

15. Kempannagari A. K., Buruju R. R., Naramgari S., & Vangala S. Effect of Joule heating on MHD non-Newtonian fluid flow past an exponentially stretching curved surface. Heat Transfer, 49(2020), 3575–3592.

16. Choi S. U. S. Enhancing thermal conductivity of fluids with nanoparticles. ASME-Publ.-Fed. 231, 99–105 (1995).

17. Haq R.U., Khan Z.H., Khan W.A., Thermophysical effects of carbon nanotubes on MHD Flow over a stretching surface, Phys. E Low-dimens. Syst. Nanostruct. 63 (2014), 215–222.

18. Rehman F., Khan M.I., Sadiq M., Malook A., MHD Flow of carbon in micropolar nanofluid with convective heat transfer in the rotating frame, J. Mol. Liq. 231 (2017), 353–363.

19. Mahanthesh B., Gireesha B.J., Animasaun I.L., Muhammad T., Shashikumar N.S., MHD Flow of SWCNT and MWCNT nanoliquids past a rotating stretchable disk with thermal and exponential space dependent heat source, Phys. Scr. 94 (2019), 1–15.

20. Hosseinzadeh K., Asadi A., Mogharrebi A.R., Khalesi J., Mousavisani M., Ganji D.D., Entropy generation analysis of (CH2OH)2 containing CNTs nanofluid flow under effect of MHD and thermal radiation, Case Studies in Thermal Engineering, 14 (2019), 1–13.

21. Ding Y., Alias H., Wen D., Williams R.A.. Heat transfer of aqueous suspensions of carbon nanotubes (CNT nanofluids), Int. J. of Heat and Mass Transfer, 49 (2006) 240–250.

22. Akbar N.S., Raza M., Ellahi R., Influence of induced magnetic field and heat flux with the suspension of carbon nano-tubes for the peristaltic Flow in a permeable channel, J. of Magnetism and Magnetic Materials. 381 (2015), 405415. https://doi.org/10.1016/j.jmmm.2014.12.087

23. Gabli A., Kezzar M., Zighed L., Sari M.R., Tabet I., Simultaneous Impacts of Fe3O4 Particles and Thermal Radiation on Natural Convection of Non-Newtonian Flow Between Two Vertical Flat Plates Using ADM, J. Non-Equilib. Thermodyn. 45 (2) (2020), 1–17.

24. Nadeem S., Abbas N., Khan A.U., Characteristics of three dimensional stagnation point flow of Hybrid nanofluid past a circular cylinder, Results in physics. 8(2018), 829–835.

25. Chamkha A.J., Dogonchi A.S., Ganji D.D., Magneto-hydrodynamic Flow and heat transfer of a hybrid nanofluid in a rotating system among two surfaces in the presence of thermal radiation and Joule heating, AIP Advances, 9(2) (2019), 025103.

26. Sundar L.S., Singh M.K., Ferro M. C., Sousa A.C., Experimental investigation of the thermal transport properties of graphene oxide/Co3O4 hybrid nanofluids, Int. Communs. in Heat and Mass Transfer. 84 (2017), 1–10.

27. Wei B., Zou C., Yuan X., Li X., Thermo-physical property evaluation of diathermic oil based hybrid nano-fluids for heat transfer applications, Int. J. of Heat and Mass Transfer. 107 (2017), 281–287. https://doi.org/10.1016/j.ijheatmasstransfer.2016.11.044

28. Momin G., Experimental Investigation of Mixed Convection with Water-Al2O3 and Hybrid Nanofluid in Inclined Tube for Laminar Flow, Int. J. Sci. Tech. Res. 2 (2014) 193–202.

29. Sundar L.S., Singh M.K., and Sousa A.C.M., Enhanced Heat Transfer and Friction Factor of MWCNTFe$_3$O$_4$/Water Hybrid Nanofluids, Int. Comm. Heat Mass Transfer, 52 (2014) 73–83.

30. Mabood F., Ashwinkumar G. P., & Sandeep N. Simultaneous results for unsteady flow of MHD hybrid nanoliquid above a flat/slendering surface. Journal of Thermal Analysis and Calorimetry, 2020, 1–13.

31. Ashwinkumar G. P. Heat and mass transfer analysis in unsteady MHD flow of aluminum alloy/silver-water nanoliquid due to an elongated surface. Heat Transfer. 2020.

32. Mabood F., Ashwinkumar G. P., & Sandeep N. Effect of nonlinear radiation on 3D unsteady MHD stag-nancy flow of Fe$_3$O$_4$/graphene–water hybrid nanofluid. International Journal of Ambient Energy, 2020, 1–11.

33. Sulochana C., & Ashwinkumar G. P. Impact of Brownian moment and thermophoresis on magnetohy-drodynamic flow of magnetic nanofluid past an elongated sheet in the presence of thermal diffusion. Multidiscipline Modeling in Materials and Structures, 2018.

34. Saba F., Ahmed N., Khan U., Mohyud-Din S.T., A novel coupling of (CNT-Fe3O4/H2O) hybrid nanofluid for improvements in heat transfer for Flow in an asymmetric channel with dilating/squeezing walls, Int. J. of Heat and Mass Transfer. 136 (2019), 186–95.

35. Xue Q.Z., Model for thermal conductivity of carbon nanotube-based composites, Physica B: Condensed Matter. 368 (2005), 302–307.

36. Hayat T., Haider F., Muhammad T., Alsaedi A., Numerical treatment for Darcy-Forchheimer Flow of car-bon nanotubes due to an exponentially stretching curved surface, Journal of Central South University. 26(4) (2019), 865–872.

37. Hayat T., Haider F., Muhammad T., Alsaedi A., Numerical study for Darcy-Forchheimer Flow of nano-fluid due to an exponentially stretching curved surface, Results in Physics. 8 (2018), 764–771. https://doi.org/10.1007/s11771-018-3947-9

38. Javed M., Farooq M., Ahmad S., Anjum A., Melting heat transfer with radiative effects and homoge-neous heterogeneous reaction in thermally stratified stagnation flow embedded in porous medium, J. of Central South University. 25 (2018) 2701–2711.

39. Okechi N.F., Jalil M., Asghar S., Flow of viscous fluid along an exponentially stretching curved surface, Results in Physics. 7 (2017), 2851–2854.

40. Liao S.J., An optimal homotopy-analysis approach for strongly nonlinear differential equations, Com-mun. Nonlinear Sci. Numer Simul. 15 (2010), 2003–2016.

41. Liao S.J., Ed. Advances in the Homotopy Analysis Method, chapter 7, " World Scientific Press" (2013).

42. Gul T., Ferdous K., The experimental study to examine the stable dispersion of the graphene nanoparti-cles and to look at the GO–H2O nanofluid Flow between two rotating disks, Appl Nanoscience. 8 (2018), 1711–1728.